A comparison of MoO_3 nanorods and C/MoO_3 nanocomposites for high-performance supercapacitor electrode

Q. Li[a], Y. F. Zhang[b,*], X. R. Han[a], C. Ju[b], Z. L. Wang[b]
[a]*School of Material Science & Engineering, Qilu University of Technology*
Shandong Academy of Sciences, Jinan, Shandong, 250353, PR China
[b]*School of Mechanical & Automotive Engineering, Qilu University of Technology*
Shandong Academy of Sciences, Jinan, Shandong, 250353, PR China

In the present work, uniform nanorods-like MoO_3 and C/MoO_3 nanocomposite were successfully synthesized through a facile hydrothermal method for high-performance electrochemical capacitors. The crystal structure and morphology of the products were characterized by X-ray diffraction (XRD) and scanning electron microscope (SEM). The electrochemical properties of the sample were tested by means of cyclic voltammetry (CV), galvanostatic charge-discharge (GCD) and electrochemical impedance spectroscopy (EIS). The C/MoO_3 nanocomposite displayed good electrochemical performance as a supercapacitor electrode material. The specific capacitance reached 115 F/g at a current density of 0.5 A g^{-1} in 6 M KOH solution. The specific capacitance of pure MoO_3 electrode only has 59 F/g at a current density of 0.5 A g^{-1}. These results represent that the C/MoO_3 nanocomposite is a promising electrode material in Supercapacitors.

1. Introduction

Supercapacitor, also known as electrochemical capacitors, is a new energy storage device with good development prospect, which has many unique advantages such as long service lifetime, high power density, fast charging–discharging rates, excellent cycle stability and so on [1-3]. Therefore, it has been attracting extensively attention in the recent years and has been gradually applied in a variety of fields including portable electronic equipment, energy backup system, hybrid electric vehicles, digital telecommunication system, etc. In general, supercapacitors can be classified into two main categories according to the charge-storage mechanism, including (i) electrical doublelayer capacitors (EDLCs), which are associated with the electrostatic charge storage mechanism that only physical reactions occur on the interface of capacitor electrodes and (ii) pseudocapacitors (PCs), which are based on a fast and reversible faradaic redox reactions mechanism, have higher specific capacitance than EDLCs due to the fast redox reaction at the electrode surfaces[4,5]. Carbon nanomaterials with large specific surface area and great electrical conductivity, including activated carbon (AC) [6], carbon nanotube (CNT) [7], graphene oxide [8], etc.

---

are the typical electrode materials for EDLCs. However, the disadvantages of low energy density and capacitance limit its development in practical applications. For PCs with a higher specific capacitance and energy density, transition-metal oxides, transition-metal hydroxides, conductive polymers, etc. are intensively used as electrodes, such as RuO_2 [9], MnO_2 [10], MoO_3 [11], PANI [12], and PPy [13], etc.

Among the various kinds of active materials for supercapacitor, MoO_3 has been widely investigated because their redox reactions enable high specific capacitances which is attributable to the mixed valence states of Mo. Pure MoO_3 can exist in three polymorphs, which include the thermodynamically stable orthorhombic phase (α-MoO_3), the metastable monoclinic (β-MoO_3) phase and the hexagonal (h-MoO_3) phase [14]. However, their low stabilities and the poor conductivities restrict the performance of supercapacitors made from them. To overcome these shortcomings, it was carried out that combining MoO_3 with conductive carbon-based material. For example, Jung et al. studied the electrochemical performances of α-MoO_3/CNTs hetero-nanostructures.[15] Zhou et al. demonstrated that the α-MoO_3/graphene nanocomposites were studied for electrochemical energy storage supercapacitor devices. [16] Noh et al. reported the carbon fiber/MoO_3 as the negative electrode in a fiber-shaped asymmetric supercapacitor (ASC) device [17]. Glucose is a cheap product that is easy to obtain and can provide carbon.
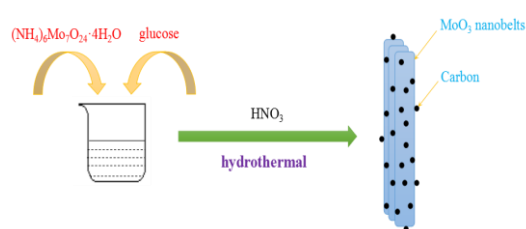
Fig. 1. Schematic illustration of the formation of the C/MoO₃ hybrid nanostructures.

Herein, we demonstrate the preparation of the C/MoO_3 nanocomposite using the glucose and the $(NH_4)_6Mo_7O_{24}$ as the carbon source and the Mo source, respectively, as shown in Figure 1. Such nanocomposites can perform as an advanced electrode material for supercapacitors and deliver a higher capacitance than that of the pure MoO_3.

2. Experimental

2.1. Materials

Ammonium molybdate ($(NH_4)_6Mo_7O_{24}$ were supplied by Shanghai Mclean Biochemical Technology Co. Ltd. Nitric acid (HNO_3) were supplied by Xintian Shuangcheng Chemical Reagent Co. Ltd. Glucose supplied by Tianjin Hengxing Chemical Reagent Co. Ltd. All the chemicals used in the experiment were of analytical grade and used without any further purification.

2.2. Synthesis of MoO₃ nanorods

The MoO_3 were prepared by a facile one-step hydrothermal method. $(NH_4)_6Mo_7O_{24} \cdot 4H_2O$ and nitric acid (HNO_3, 68 wt %) were used as raw materials. Typically, 1 g ammonium molybdate

was dissolved in 30 mL distilled water under vigorous stirring to form a homogeneous solution. Then, 6 mL HNO_3 (68 wt %) solutions were added to the solution with constant magnetic stirring for 30 min. After that, the mixtures were transferred into a 100 mL Teflon-lined stainless-steel autoclave and heated at 220 ^oC for 24 h. While the autoclave naturally cooled down to room temperature, the product was collected by centrifugation, rinsed with distilled water and absolute ethanol for several times, and then dried in vacuum at 80 °C for 12 h.

2.3. Preparation of C/MoO₃ composites

1 g $(NH_4)_6Mo_7O_{24} \cdot 4H_2O$ and 0.25 g glucose were added and dissolved in 30 mL distilled water under magnetic stirring, following adding 6 mL HNO_3 (68 wt%) solutions to the solution and continuously stirring for 30 min. Next, the solution was transferred into a 100 mL Teflon-lined stainless-steel autoclave, which was heated to 220 ^oC and held for 24 h. After being cooled down to room temperature, the precipitate was washed with distilled water and absolute ethanol for several times, following by drying in vacuum at 80 °C for 12 h.

2.4. Material characterization

The structure, morphology and electrochemical properties of the material were characterized at room temperature by a variety of means. X-ray diffraction (XRD) patterns of the as-synthesized MoO_3 and C/MoO_3 nanocomposites were conducted on an X Pert PRO MPD diffractometer (PANalytical B.V, Netherlands) operated at 40 KeV and 40 mA with a Cu Ka radiation ($\lambda = 0.15418$ nm) in the range of 10–60°. Scanning electron microscope (SEM) images were obtained on a FEISirion200 (Philips, Netherlands).

The electrochemical measurements of supercapacitors were taken in 1 M NaOH aqueous solution as electrolyte using a conventional three-electrode system setup (VMP3, BIO-LOGIC, France) consisting of a Platinum (Pt) sheet as counter electrode, a saturated calomel electrode (SCE) as reference electrode and the as-synthesized material-based electrode as the working electrode. The cyclic voltammetry (CV) measurements of supercapacitors were carried out at different scan rate from 10 to 100 mVs^{-1} in the potential rage of 0-0.6 V. The galvanostatic charge-discharge (GCD) tests were taken in different current densities from 0.5 to 2 A g^{-1} in 6 M KOH electrolyte. The electrochemical impedance spectroscopy (EIS) measurements were also conducted in the frequency range from 10 mHz to 100 kHz.

The working electrodes were fabricated by mixing the active material, carbon black and PTFE with the mass ratio of 80:10:10. Then, the mixture was pressed onto the nickel foam current collector (5 mg cm^{-2}) and dried at 60 $^{\circ}C$ for 12 h. The specific capacitance (C) of electrode material can be calculated from the galvanostatic charge-discharge curve according to equation (1):

$$C = \frac{I\Delta t}{\Delta Vm} \tag{1}$$

where C (F g^{-1}) is the specific capacitance, I (A) is the current, Δt (s) is the discharge time, ΔV (V) is the potential window, and m (g) is the mass of the electroactive material.

3. Results and discussion

3.1. Material characterization

The crystal structure and phase purity of the MoO_3 were characterized by X-ray powder diffraction (XRD). Figure 2 shows the XRD pattern of the MoO_3 nanostructure sample. The peaks at 12.8, 23.7, 25.8, 27.4, 33.7, 39.1, 46.3 and 59.1 correspond to (001), (101), (002), (011), (110), (102), (201) and (114), respectively. It could be seen that nearly all the diffraction peaks in the XRD pattern are in agreement with the standard structure (JPCDS no. 47-1320) of the MoO_3 nanorods and no excrescent characteristic peaks are detectable in the XRD pattern, indicating that pure MoO_3 nanorods were successfully synthesized.
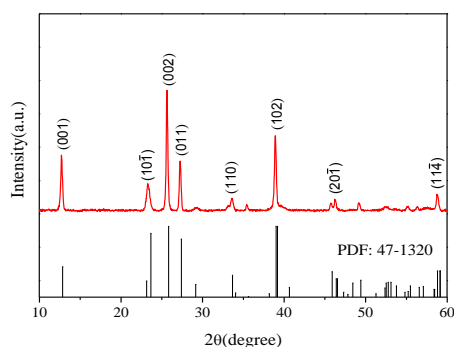
Fig. 2. XRD patterns of the pure MoO₃ nanorods and standard card.

The morphology of the as-prepared pure MoO_3 and C/MoO_3 samples was characterized by SEM analysis as shown in Figure 3. The low and high magnification SEM images of the pure MoO_3 nanorods were shown in Figure 3 (a, b). From Figure 3 (a, b), it can be observed that the as-prepared MoO_3 nanorods have a uniform morphological distribution with smooth surface. The pure MoO_3 nanorods was 2-8 μm in length, and 300-500 nm in diameter. The large specific area is beneficial to energy storage devices. Figure 3 (c, d) shows the low and high magnification SEM images of the C/MoO_3 nanocomposites. In the C/MoO_3 nanocomposites, the carbon attached to the MoO_3 nanorods.
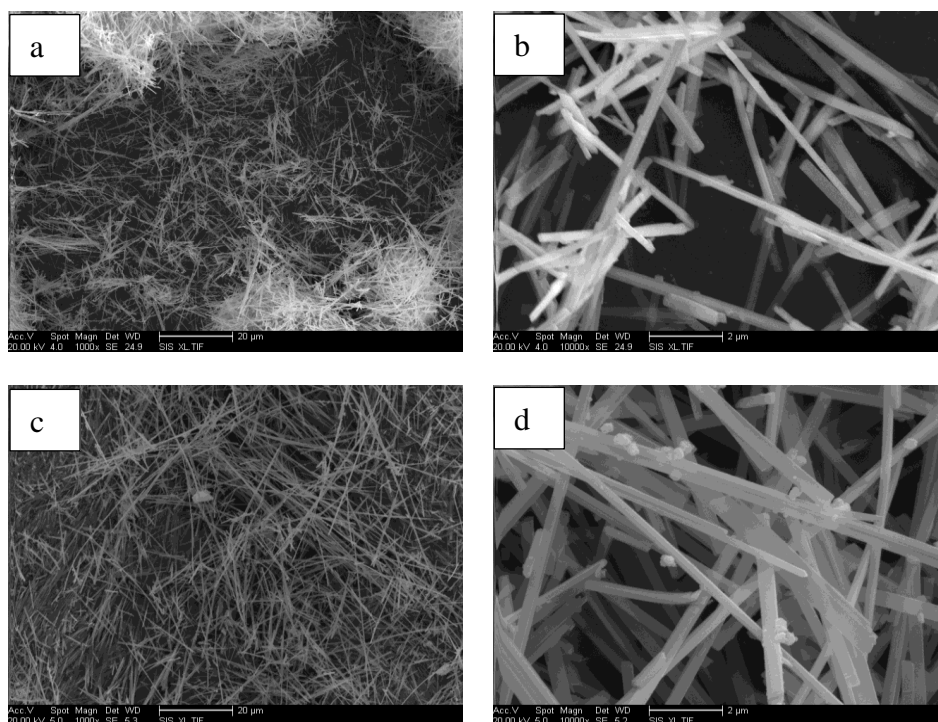
Fig. 3. (a, b) Low- and high-magnification SEM images of the pure MoO$_3$ nanorods. (c, d) Low- and high-magnification SEM images of the C/MoO$_3$ nanocomposites.

3.2. Electrochemical performance

The cyclic voltammetry (CV), galvanostatic charge-discharge (GCD) and electrochemical impedance spectra (EIS) tests were carried out to evaluate the electrochemical performance of the obtained material.
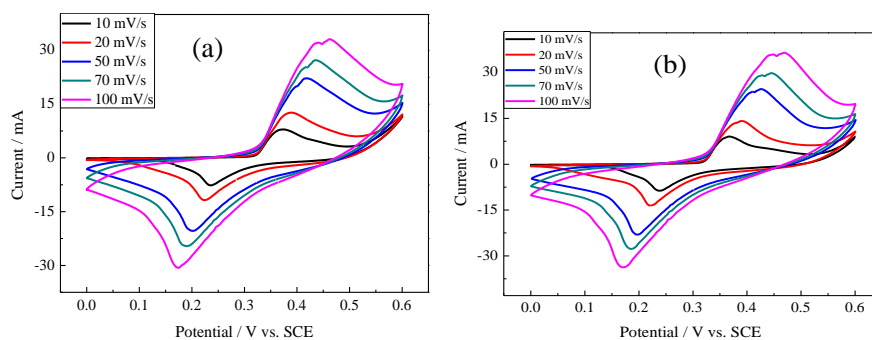
Fig. 4. (a) CV curves of the pure MoO$_3$ at the different scan rates. (b) CV curves of the C/MoO$_3$ nanocomposites at the different scan rates.

The CV curves of the pure MoO$_3$ and the C/MoO$_3$ nanocomposites at the different scan rates were shown in Figure 4a and b. The CV shapes of the two kinds of electrode materials were both of pseudocapacitance type. It was observed that an obvious pair of redox peaks attributed to the reversible oxidation state change of Mo element between Mo (IV) and Mo (VI) [18].

With the increase of the scan rate, the shapes of CV loop were approximate, indicating that the as-prepared material has good electrochemical stability. But We can notice a phenomenon that there is obvious deviation of redox peaks in the CV shapes as the scan rate increases from 10 to 100 mV s^{-1}. This is dependent upon the electrode and electrolyte resistance, and is related to the scan rates.
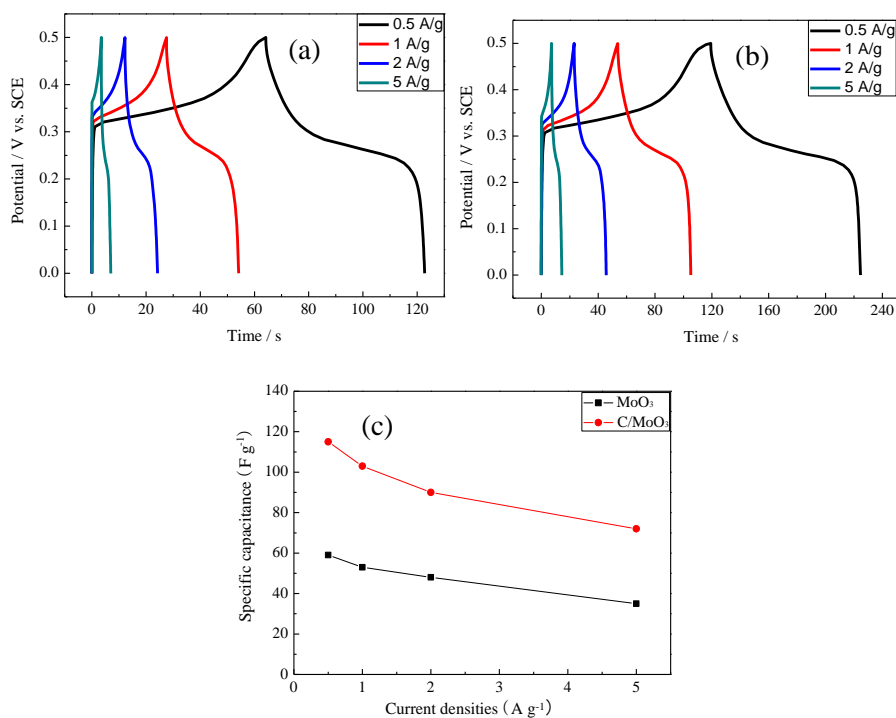
Fig. 5. (a) Galvanostatic charge−discharge curves of the pure MoO$_3$ at the different current densities. (b) Galvanostatic charge−discharge curves of the C/MoO$_3$ nanocomposites the different current densities. (c) The corresponding specific capacitance of pure MoO$_3$ and C/MoO$_3$ nanocomposites at different current densities.

It was important to calculate accurately the specific capacitance and further evaluate the electrochemical performance of electrode materials by galvanostatic charge-discharge curves of the electrode. The GCD curves of the pure MoO$_3$ and the C/MoO$_3$ nanocomposites at the different current densities in the potential rage of 0-0.5 V were shown in Figure 5a and b. They are the type curves of pseudocapacitors, again implying the ideal capacitive characteristic. The corresponding C_s values were calculated based on Equation (1). As expected, the C/MoO$_3$ nanocomposites achieves the highest specific capacitance (115 F g^{-1}) than the specific capacitance (59 F g^{-1}) of the MoO$_3$ electrode at a current density of 0.5 A g^{-1}. Such a phenomenon could be attributed to the following the reason: the amorphous carbon in composite materials facilitates the electrons transport during the processes of charging and discharging because of its high conductivity. As shown in Figure 5c, the specific capacitances of the C/MoO$_3$ nanocomposites evaluated from GCD curves at current densities of 0.5, 1, 2, 5 A g^{-1} were 115, 103, 90, 72 F g^{-1}, respectively. The specific capacitances of the MoO$_3$ were 59, 53, 48, 35 F g^{-1} at current densities of 0.5, 1, 2, 5 A g^{-1}, respectively, which are lower than the specific capacitances of the C/MoO$_3$ nanocomposites at same current densities.
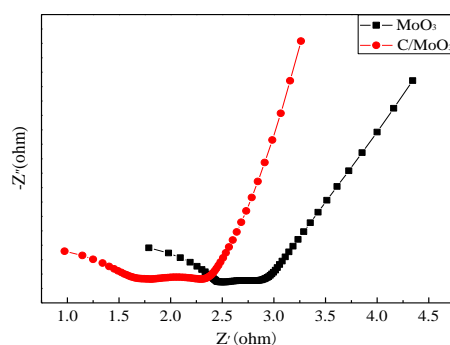
Fig. 6. The Nyquist plots of the MoO$_3$ and C/MoO$_3$ electrodes.

The electrochemical properties of the as-prepared samples could be further studied by the electrochemical impedance spectroscopy (EIS) measurements as shown in Figure 6. The Nyquist plots are composed of a semicircle in the high-frequency range where the diameter of the semicircle represents the charge-transfer resistance (R$_{ct}$) at the electrode/electrolyte interface, and a straight line in the low-frequency range where the slope of a straight line is related to the diffusive resistance of the electrolyte into the interior of the electrode and the ion diffusion into the electrode. In comparison with the slope of the MoO$_3$, the slope of the C/MoO$_3$ nanocomposite is higher, implying it possesses the smallest resistance.

4. Conclusion

In summary, MoO$_3$ nanorods with 2-8 μm in length and C/MoO$_3$ nanocomposites have been successfully fabricated via a hydrothermal method. The crystal structure and morphology of the MoO$_3$ have been characterized by XRD and SEM. Electrochemical measurements indicate that the C/MoO$_3$ nanocomposites electrode exhibited a higher specific capacitance (115 F g^{-1} at current densities of 0.5 A g^{-1}) than the pure MoO$_3$ electrode. The promising electrochemical properties were attributed to the addition of C which can increase the conductivity of material. From these results, it was demonstrated to their promising capability as a supercapacitor electrode.

References

[1] Y. Zheng, Y. B. Yang, S. S. Chen et al., Crystengcomm. **18**, 4218 (2016).
[2] P. M. Shafi, R. Dhanabal, A. Chithambararaj et al., Acs Sustainable Chemistry & Engineering

5, 4757 (2017).

[3] S. Wang, K. Dou, Y. Dong et al., International Journal of Nanomanufacturing **12**, 404 (2016).

[4] S. Sun, X. Liao, Y. Sun et al., Rsc Advances **7**, 22983 (2017).

[5] V. Kumar, P. S. Lee, Journal of Physical Chemistry C **119**, 9041 (2015).

[6] L. H. Yin, Y. Chen, D. Li et al., Materials & Design **111**, 44 (2016).

[7] P. Sun, H. Yi, T. Q. Peng et al., Journal of Power Sources **341**, 27 (2017).

[8] R. Kumar, R. K. Singh, A. R. Vaz et al., ACS Applied Material & Interfaces **9**, 8880 (2017).

[9] J. Y. Hwang, M. F. El-Kady, Y. Wang et al., Nano Energy **18**, 57 (2015).

[10] H. M. Wei, J.. X Wang, S. W. Yang et al., Journal of Electronic Materials **46**, 1539 (2017).

[11] F. Barzegar, A. Bello, D. Y. Momodu et al., Rsc Advances **5**, 37462 (2015).

[12] H. H. Wang, L. Ma, M. Y. Gan et al., Journal of Alloys & Compounds **699**, 176 (2017).

[13] X. Jian, J. G. Li, H. M. Yang et al., Carbon **114**, 533 (2017).

[14] R. Liang, H. Cao, D. Qian, Chemical Communications **47**, 10305 (2011).

[15] H. Jung, B. Kim, S. Kim et al., Materials Letters **204**, 173 (2017).

[16] J. H. Zhou, J. Song, H. H. Li et al., New Journal of Chemistry **39**, 8780 (2015).

[17] J. Noh, C. M. Yoon, K. K Yun et al., Carbon **116**, 470 (2017).

[18] X. Cao, B. Zheng, W. Shi et al., Advanced Materials **27**, 4695 (2015).